Available online at www.sciencedirect.com
ScienceDirect
Earth and Planetary Science Letters 254 (2007) 9–27
EPSL
www.elsevier.com/locate/epsl

Rupture lengths and temporal history of significant earthquakes on the offshore and north coast segments of the Northern San Andreas Fault based on turbidite stratigraphy

Chris Goldfinger [a,*], Ann E. Morey [a], C. Hans Nelson [b], Julia Gutiérrez-Pastor [b], Joel E. Johnson [a,1], Eugene Karabanov [c], Jason Chaytor [a], Andrew Eriksson [a]
Shipboard Scientific Party

[a] *Oregon State University, College of Oceanic and Atmospheric Sciences, 104 Ocean Admin. Bldg., Corvallis OR 97331, USA*
[b] *Instituto Andaluz de Ciencias de la Tierra (IACT) CSIC-Univ. de GranadaCampus de Fuentenueva s/n 18002 Granada, Spain*
[c] *University of South Carolina, Department of Geological Sciences, Columbia, SC, 29208, United States*

Received 21 July 2006; received in revised form 6 November 2006; accepted 10 November 2006
Available online 4 January 2007
Editor: R.D. van der Hilst

Abstract

74 piston, gravity and jumbo Kasten cores were collected from channel and canyon systems draining the northern California continental margin to investigate the record of periodic Holocene turbidites for possible connection to large magnitude earthquakes on the adjacent Northern San Andreas Fault. Poorly known channel systems were mapped with multibeam sonar to define pathways and channel confluences. Cores sampled all major and many minor channel systems extending from Cape Mendocino to just north of Monterey Bay. Sampling both along and across channels was done and particular attention was paid to channel confluences, as these areas afford opportunities to test for synchronous triggering of turbidity currents. While at sea, all cores were scanned using a GEOTEK multisensor core logger (MSCL), which collects high-resolution photography, P-wave velocity, gamma-ray density, and magnetic susceptibility data from the unsplit cores. Lithology was logged visually, and cores were later imaged with X-radiography.

We use ^{14}C ages, relative dating tests at channel confluences, and stratigraphic correlation using physical properties to determine whether turbidites deposited in separate channel systems are correlative, implying they were triggered by a common event. These tests can, in most cases, separate earthquake-triggered turbidity currents from other possible sources. The late Holocene turbidite record off northern California passes these tests for synchronous triggering, and can be correlated with multiple proxies from site to site between Noyo Channel and the latitude of San Francisco. Preliminary comparisons of our event ages with existing and in progress work at onshore coastal sites show good correlation, further circumstantial evidence that the offshore record is primarily earthquake generated. During the last ~2800 yr, 15 turbidites are recognized, including the great 1906 earthquake. Their chronology establishes an average repeat time of ~200 yr, similar to the onshore value of ~230 yr. Along-strike correlation suggests that at least 8 of the youngest 10 of these events ruptured the 320 km distance from the Mendocino Triple Junction to near San Francisco.

Keywords: Paleoseismology; Turbidite; Northern San Andreas Fault

* Corresponding author. Tel.: +1 541 737 5214.
E-mail addresses: gold@oregonstate.edu (C. Goldfinger), odp@ugr.es (C.H. Nelson), juliagp@ugr.es (J. Gutiérrez-Pastor).
[1] Present address: University of New Hampshire, Department of Earth Sciences 56 College Rd. Durham, NH 03824 3589.

0012-821X/$ - see front matter © 2006 Published by Elsevier B.V.
doi:10.1016/j.epsl.2006.11.017

1. Introduction

Recent rapid advances in Global Positioning System (GPS) technology now make it possible to measure crustal strain accumulation at plate boundaries with a high degree of certainty in only a few years. However, real-time strain measurements typically represent a fraction of one strain cycle. Fundamental questions about clustering, the applicability of slip-predicable or time-predicable models and the nature of long term stress interactions (e.g. [1,2]) remain largely unanswered because we rarely have a long enough earthquake record. What is needed most is recurrence data for more fault systems and over longer spans of time, so that meaningful statistical conclusions can be drawn. Paleoseismology has the potential to address these questions by directly using the larger time span available through the geologic record and precise dating techniques. In the past decade, discovery of rapidly buried marsh deposits and associated tsunami sands along the northern Pacific Coast of the US has led to the recognition that the Cascadia subduction zone, once thought aseismic due to low instrumental seismicity, has generated great (Mw 8–9) earthquakes in the past (e.g. [3,4]) and spurred the development of *off-fault* paleoseismology.

We have been using the marine turbidite record as a proxy for earthquake recurrence in both Cascadia and on the Northern San Andreas Fault (NSAF) [5,6]. Turbidite paleoseismology and other off-fault techniques must of course demonstrate that the events recorded are earthquake-triggered. Marine records are more continuous and extend further back in time than land records in most cases, and are actually more precise in the early to mid Holocene due to the abundance of datable foraminifera. In recent years, turbidite paleoseismology has been attempted in Cascadia [5–7], Puget Sound [8], Japan [9–11], the Mediterranean [12], the Dead Sea [13], northern California [14,15] and the Arctic ocean [16], and is a technique that is evolving as a precise tool for seismotectonics.

In 1999–2002, we collected 74 piston, gravity and jumbo Kasten cores from channel/canyon systems draining the northern California margin adjacent to the onshore and nearshore NSAF (Fig. 1). We mapped channel systems with a Simrad EM-120 multibeam sonar, collecting both high-resolution bathymetry and backscatter data essential for analysis of channel morphology, sedimentation patterns, and core siting. These data were processed and merged with existing multibeam data.

During the cruise, we sampled all major and many minor channel systems extending from Cape Mendocino to just north of Monterey Bay (Fig. 1). Sampling both down and across channels in some cases was done, and particular attention was paid to channel confluences, as these areas afford opportunities to test for synchronous triggering of turbidity currents.

These cores have yielded a turbidite record that is in good agreement with the shorter land record of Holocene NSAF earthquakes. Despite the intense scientific study of the NSAF stemming from the great seismic hazards to San Francisco, a reliable event history for this fault extending back through the Holocene has yet to be established. This is particularly true for the segments of the NSAF near and north of San Francisco. Establishment of an offshore record, reconciled with the land paleoseismic record, offers the opportunity to investigate long term earthquake behavior, stress interactions with other fault systems, and enables the use of these parameters in probabilistic hazard models.

In this paper we present preliminary results from the offshore turbidite event record along the NSAF extending to ~3000 ybp. We detail results from multiple tests of synchronous triggering, a key requirement for earthquake origin, as well as a comparison with onshore paleoseismic data. Finally, we examine the origins of detailed stratigraphic correlations, and the potential for extracting earthquake rupture information from the stratigraphic record.

2. Geological setting and background

2.1. NSAF seismotectonic setting

The San Andreas Fault (SAF) is probably the most intensively studied transform system in the world. Extending along the west coast of North America, from the Gulf of California to Cape Mendocino, the SAF is the largest component of a complex and wide plate boundary that extends eastward to encompass numerous other strike–slip fault strands and interactions with the Basin and Range extensional province. The Mendocino Triple Junction (MTJ) lies at the termination of the Northern San Andreas, and has migrated northward since about 25–28 Ma [17]. As the triple junction moves, the former subduction forearc transitions to right lateral transform motion and the SAF continues to lengthen.

West of the Sierra Nevada block, three main fault systems accommodate ~75% of the Pacific–North America plate motion, distributed over a 100 km wide zone [18]. The Eastern California Shear Zone carries the remaining plate motion [18,19]. The NSAF accommodates about 25 mm/yr of the ~34 mm/yr distributed

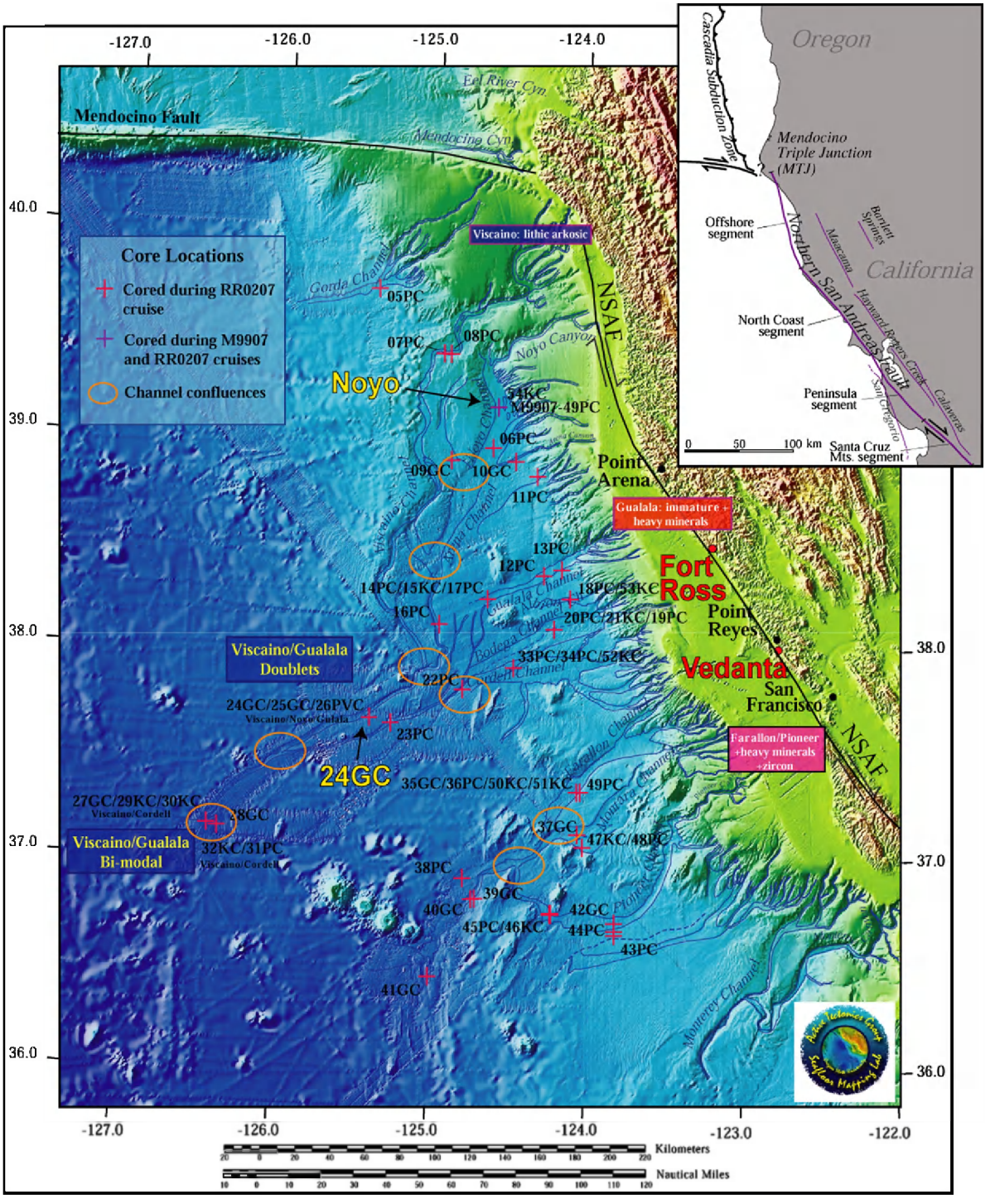

Fig. 1. Core locations from 1999 and 2002 cruises on R/V Melville and Roger Revelle. Bathymetric and topographic data compiled by OSU from NASA land data, archive and newly collected marine survey data during these cruises. Channel systems were mapped from the new bathymetric grid and sidescan data. Core numbers are referred to in the text. Noyo Cores (including 49PC from Melville 1999 cruise) and 24GC, discussed in text are also shown in yellow. Offshore provenance from heavy mineral analyses are indicated in boxed text. At the confluence upstream of 24GC, Viscaino and Gualala mineralogies mix and result in stacked pulses, reflecting source mineralogies. Onshore paleoseismic sites Vedanta and Fort Ross are shown in red.

across northwestern California. Most of the remainder is taken up on the parallel Hayward–Rogers Creek, Calaveras, Maacama and Bartlett Springs Faults (Fig. 1). South of San Francisco, the NSAF bifurcates to include the San Gregorio Fault, joining the Northern San Andreas at Olema. Between San Francisco and Cape Mendocino, the main strand of the San Andreas is a relatively simple system. Several uncertain faults exist offshore, but the age and activity of these faults is unknown [20]. Since the 1906 rupture, the main NSAF has been nearly aseismic [21], with only a few small events near Pt. Arena. Seismicity has been greater near the MTJ, and on the Maacama and Bartlett Springs faults to the east [22].

2.2. Northern San Andreas onshore paleoseismicity

The NSAF system has been divided into segments based on its historical record of earthquake behavior. All four northern segments (north of the creeping section at San Juan Bautista: Santa Cruz Mountain, Peninsula, North Coast, and Offshore [23]) ruptured in the 1906 Mw 7.9 earthquake, extending from the San Juan Bautista north to the Mendocino Triple Junction [24–26]. The minimum rupture length for this event is estimated to be ~470 km [27].

The paleoseismology of the NSAF has been investigated at Olema, 45 km north of San Francisco, at Dogtown, close to the Olema site, at Point Arena, Fort Ross, at several sites on the San Francisco Peninsula, and at Arano and Grizzly Flats in the Santa Cruz mountains. At the Vedanta site (Fig. 1) near Olema, Niemi and Hall [28] found a maximum late Holocene slip rate of 24±3 mm/yr, in fair agreement with geodetic data [29]. They estimate that if the 4–5 m slip event recorded in 1906 is characteristic, the recurrence time for such events would be 221±40 yrs. The average slip per event at Point Arena similarly implies a recurrence time of 200–400 yrs [30]. Recently, 10 new ages from the Vedanta site [31] and sites near Fort Ross [32] (Fig. 1), suggest a recurrence interval of ~230 yr, and timing of the penultimate event on the North Coast and Offshore segments at ~AD 1700–1750.

A controversial aspect of NSAF tectonics has been whether the fault is seismically segmented, or whether the long 1906 rupture was characteristic, or perhaps a mix of both. The consistent slip rates found north of the Golden Gate, slow to about 17 mm/yr south of the Golden Gate. This, and a lower 1906 co-seismic slip south of the Golden Gate [33–35] led investigators to conclude that the fault is segmented near the Golden Gate. Schwartz et al. [27] argues that the segmentation is a reflection of the offshore San Gregorio Fault absorbing some of the slip [36,37], correspondingly reducing the slip rate on the main SAF. They argue that the through-going rupture in 1906 (and perhaps previous events) was not segmented, and further, that the penultimate event ruptured approximately the same distance and magnitude as the 1906 event. Fumal et al. [38] however, reports that the Santa Cruz Mountain segment has a more frequent recurrence interval (~100 yr) than is evident for the North Coast and Peninsula segments.

3. Turbidite methodology and analytical methods

3.1. Turbidite methodology and application to Cascadia and the San Andreas

3.1.1. Identifying earthquake-triggered turbidites

The Grand Banks earthquake of 1929 in the northwest Atlantic clearly demonstrated the association between earthquakes and turbidity currents [39], however other plausible triggers for turbidity currents include: 1) storm or tsunami wave loading; 2) sediment loading; and 3) storm (hyperpycnal) discharges. Investigators have attempted to distinguish seismic turbidites from storm, tsunami, and other deposits [9–11], arguing that seismo-turbidites can in some cases be distinguished sedimentologically. They observe that known seismically triggered turbidites in the Japan Sea and Lake Biwa (western Honshu, Japan) are distinguished by wide areal extent, multiple coarse fraction pulses, variable provenance, and greater depositional volume than events triggered by other mechanisms. These investigators observed that known earthquakes caused multiple slump events in a canyon system, generating multiple pulses resulting in an amalgamated turbidite also including reverse grading and cutouts (Fig. 2).

Similar observations regarding areal extent and volume have been made for the Santa Monica and Alfonso Basins of the California Borderland and Gulf of California respectively [40]. In general, these investigators observe that known storm sediment surges are thinner, finer grained and have simple and mostly normal over inverse graded Bouma sequences.

In this paper, we do not attempt to distinguish between triggering mechanisms sedimentologically, but use a spatial and temporal pattern of event correlations to establish synchronous triggering within individual canyons along 320 km of coastline. Synchroneity of event records in separated canyons, over a wide region, is difficult to attribute to non-earthquake sources which are mostly limited spatially and temporally to single canyons. Possible exceptions include storm wave

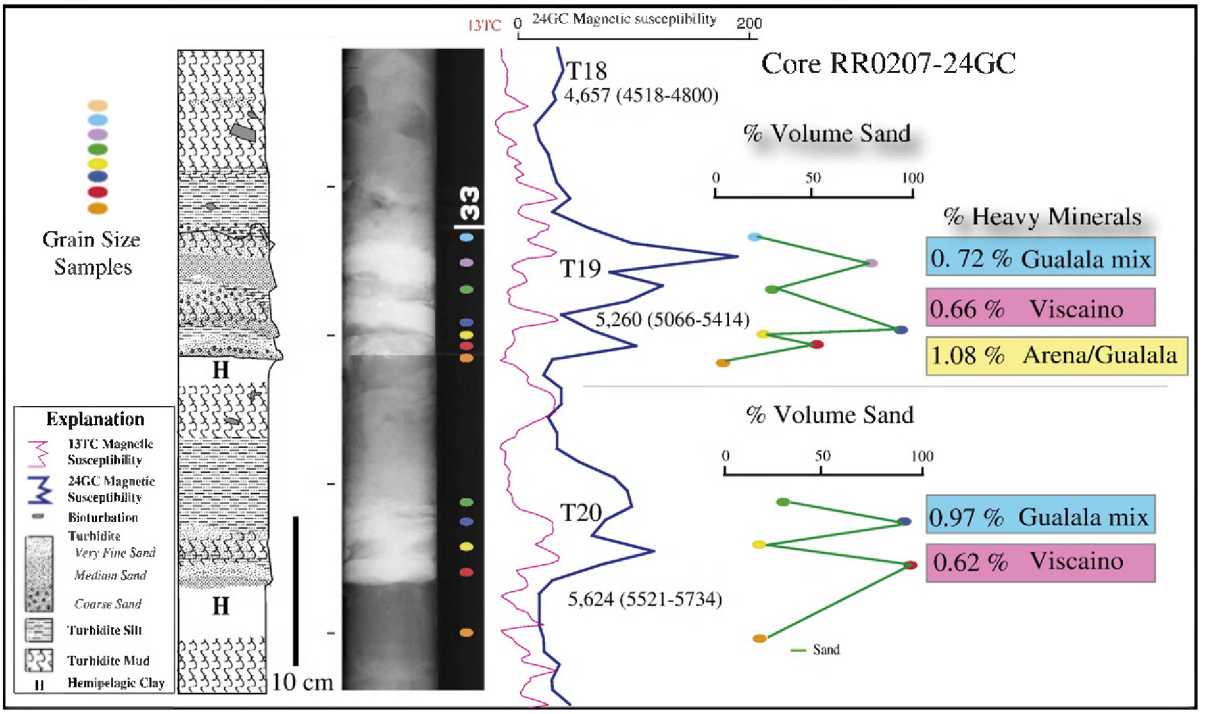

Fig. 2. Grain size analysis, magnetic susceptibility/density signatures and X- radiography in turbidites T19 and T20 in core 24GC below the Gualala–Noyo–Viscaino channel confluence (Base of T18 is also shown; see Fig. 1 for location). Light tones in the x-radiograph represent dense sand/silt intervals, darker gray tones represent clay/mud. Colored dots are grain size samples. Blue trace is the magnetic susceptibility signature. Green plot is percent sand (obtained with Coulter laser counter method). The good correspondence between grain size, density, and magnetic susceptibility for the lithologies in NSAF cores is apparent, and permits use of density and magnetics as mass/grain size proxies due to the large number of analyses that would otherwise be required. These typical turbidites are composed of 1–3 fining upward sequences, each truncated by the overlying "pulse". No hemipelagic exists between pulses, indicating the three pulses were deposited in a short time interval. Only the last pulse has a fine tail, indicating final waning of the turbidity current. We interpret these signatures as resulting from a single multipulse turbidity current. Number of coarse pulses commonly remains constant in multiple channel systems for a given event. "H" denotes hemipelagic sediment between turbidites. Correlative magnetic susceptibility trace for Gualala core 13TC is also shown, as are correlative ^{14}C ages projected from core 54KC in Noyo Channel. Source provenance affinity for each sand pulse is shown to the right, and keyed to source regions in Fig. 1. This shows the arrival of discrete source pulses with a dominant lithology from multiple channel systems.

loading and hyperpycnal flow, which also occur over large areas and short time scales.

Hyperpycnal flows, or direct turbid injections from rivers, can produce turbidity currents, and can even mimic earthquakes in that they may affect several rivers over a span of days. This certainly occurred during periods of lowered sea level during the Pleistocene, when there was direct connection between rivers and offshore canyons. However, sea level-rise in the Holocene isolated most west coast canyons from their rivers [41,42]. Holocene sediment input is generally distributed across the shelf, not directly injected in the canyons, with some narrow-shelf exceptions such as the Eel, Mendocino, Viscaino, and Monterey Canyons [43–45] (Fig. 1).

Tsunamis and storm waves may also conceivably act as regional triggers of turbidity currents. Storm waves can induce sediment resuspension by either erosion due to shear stress induced by orbital motion from the waves, or from fluidization of near surface sediments due to cyclic pressure changed during repeated wave passage. Our calculations based on [46] and using historical and predicted maximum wave data [47] suggest that extreme storm waves common in the NE Pacific have the potential to both erode and liquefy sediments at canyon head depths of ~120–150 m. Nevertheless, we see no evidence of such material reaching the abyssal plain, indeed there is nothing but hemipelagic sediment overlying the turbidite triggered by the AD 1700 Cascadia earthquake [5,6] and the 1906 NSAF event. Puig et al. [44] and other investigators have shown that this process occurs, but also that such flows generally settle in the canyons in 200–500 m depth where the resuspending force dies out. We note that the tsunami from the 1964 Alaska Mw 9.0 event also did not result in deposition of turbidites in abyssal plain channels in

Cascadia Basin [5–7]. For these reasons, it appears that synchronous widespread deposition of turbidites on the abyssal plain, at least during high sea level, is best explained by a proximal great earthquake source.

3.1.2. Tests of synchronous triggering and correlative deposition of turbidites

Unlike Cascadia, the northern California margin does not appear to have a regional stratigraphic datum like the Mazama ash deposited along the Cascadia margin [5,6], thus correlating events and testing for event origin depends heavily on stratigraphic correlation of other datums and radiocarbon ages. A key test of synchronous triggering has become known as the "confluence test". In Cascadia Basin channels, Adams [7] observed that most cores contained 13 turbidites overlying the Mazama ash (which was included in the 13th). Cores from Juan de Fuca Canyon, Willapa, Grays, and Quinault Canyons also contain 13 turbidites and include the Mazama ash (several additional events appear in the most proximal canyon sites). The correlative turbidites in Cascadia channel lie downstream of the confluence of those channels. If these events had been independently triggered, with more than a few hours separation in time, the channel(s) below the confluence should contain from 26–28 turbidites not 13 as observed. This simple observation demonstrates synchronous triggering of turbidity currents in tributaries, the headwaters of which are separated by 50–150 km. Similar inferences about regionally triggered synchronous turbidites in separate channels elsewhere have been reported [9,11,40,48].

We have begun to apply this "confluence test" to the NSAF turbidite data. In the NSAF system, channel mapping shows that there are eight major confluences available (Fig. 1). Here a modified confluence test is applied to ~6000 years of turbidite record observed in multiple systems meeting at multiple confluences. We have been able to distinguish three heavy mineral provenances in the cores, well linked to the onshore source geology (Fig. 1). Using these three heavy mineral suites allows us to distinguish the various dominant sources of the stratigraphy within turbidites both up and downstream from confluences, and test for synchronous or asynchronous arrival at confluences by observing the stacking of turbidites and their provenance components. As in the original confluence test, a sequence of turbidites should show little change in stratigraphy downstream of confluences if the multiple source canyons were triggered simultaneously, but may show the arrival and blending of the separate provenance components.

3.2. Analytical methods

3.2.1. Stratigraphic correlation and event "fingerprinting"

We carried out extensive sampling of the physical properties of the cores to establish the stratigraphy reflected in the cores. This has allowed us to identify characteristic stratigraphic "fingerprints" for turbidite sequences that are a result of the grain size distribution of individual events. Because this property has allowed stratigraphic correlation along hundreds of km of coast, we discuss the methods and implications in detail.

While at sea, all cores were scanned using a GEOTEK MSCL, collecting P-wave velocity, gamma-ray density, and magnetic susceptibility data from the unsplit cores. Cores were then split to collect high-resolution line-scan imagery. Subsequently, high-resolution magnetic susceptibility data were collected from each core using a point probe (Bartington MS2E high-resolution surface sensor) at 1 cm intervals, selected cores at 3 mm intervals, and imaged with X-radiography (e.g. Fig. 2). Selected grain size analyses were performed with a Coulter laser counter.

Initially these data were used to correlate stratigraphy between cores at single sites, which typically have 4–6 cores. This makes use of the trigger cores (collected 1 m apart from the linked piston cores), and helps identify missing upper sections, an occasional problem with piston cores. The correlation is done using primarily magnetic susceptibility (MS) and density, much as e-logs are correlated in the oil industry [49,50]. Physical property correlations of this type are also common practice with academic and ODP/IODP cores (e.g. [51]) and have recently come into use for paleoseismology (i.e. [8,52–56]). In addition to local site correlation, we have found that it is possible to correlate unique physical property signatures of individual turbidites from different sites within individual channels. This suggests that the processes controlling deposition of the turbidite maintain consistency for some considerable distance within a channel. We have also found it possible to correlate event signatures not only down individual channels and past confluences, but between channel systems separated by considerable distance, some of which never meet. These turbidite "fingerprints" form the basis of long-distance correlations, and are beginning to be recognized and used for regional correlation (e.g. Lake Baikal [57], off Morocco [58], Cascadia [59] the Laptev Sea: Russian Arctic [60] and elsewhere). Recently, the "event signatures" of Cascadia turbidites have been linked to coastal fjord records on Vancouver Island [61,62].

Fig. 2 shows a single representative turbidite in core 24GC, located below two channel confluences (Fig. 1); illustrating the multiple fining-upward sequences (Bouma A–C) that compose each turbidite. Typically, these sequences have only one fine tail (Bouma D) associated with waning of the turbidity current. The signatures we are correlating are comprised of these stacked coarse pulses. This figure shows in detail that the magnetic susceptibility, density, and grain size trends within each event are closely correlated. This is straightforward but important because we can in most cases use the high-resolution density and magnetic data as grain size proxies, at least for lithologies along the NSAF system [63–65]. In detail, the magnetic susceptibility (MS) signal is associated with terrestrial silt-sized magnetic minerals, but often we see sand at the turbidite base. The sand may be non-magnetic quartz sand, so the MS peak does not always correlate perfectly with a maximum of grain size. Also in thick turbidite beds, separation of grains according to specific gravity (or mineral density) can dominate, resulting in fine silt heavy mineral lamina located below medium quartz silt or sand. We find, however, that this approximation is reasonable in most cases (using both density and MS reduces this problem), and the differences are not critical to observing a recognizable "fingerprint" for many turbidites.

On close inspection of physical property logs, we sometimes see a remarkable similarity between correlative turbidites that are separated by as much as 500 km (Cascadia) and 280 km (NSAF). Fig. 3 shows several typical examples of correlative NSAF events in detail along strike over a distance of 280 km. We see a general correspondence of relative turbidite size downcore that is reflected in separate channels, as well as correlable details such as the number of coarse sandy pulses (density and magnetic peaks). For example, Cascadia turbidite events T5, T10, and T12 are small events in all cores, T11 and T16 are very

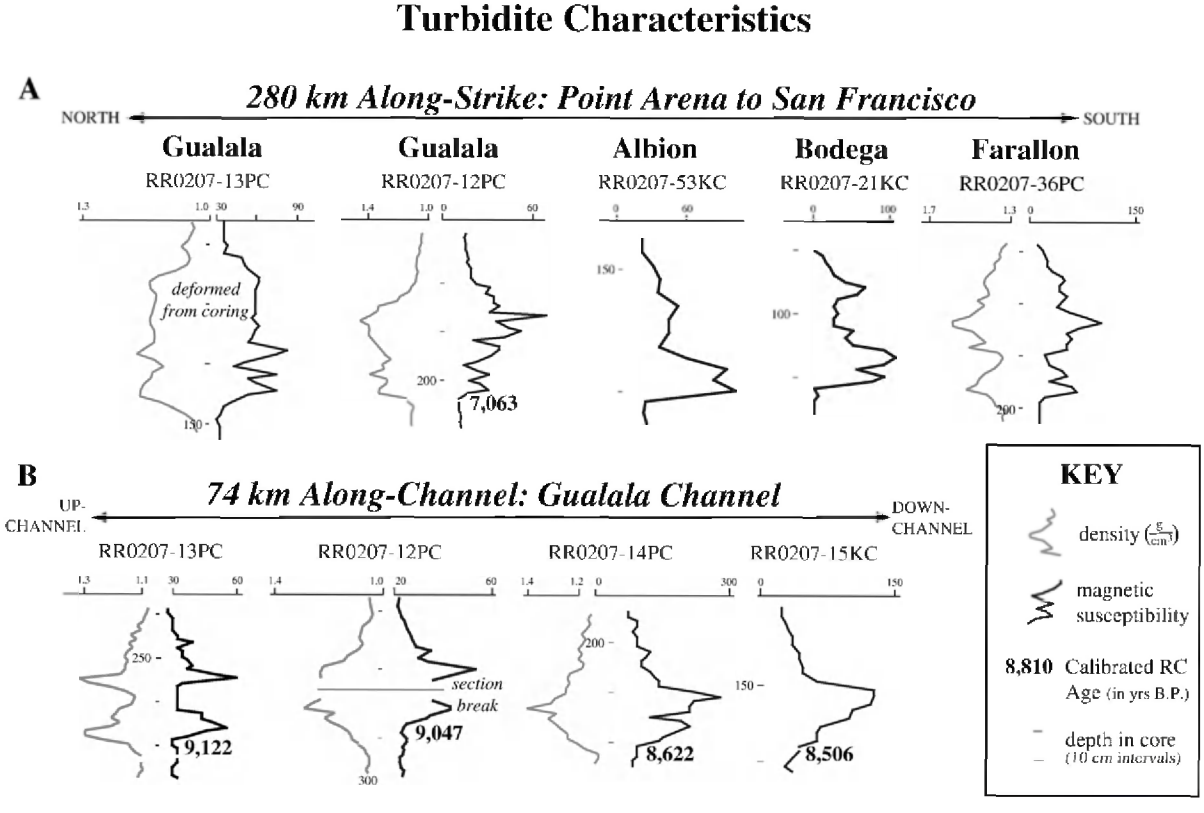

Fig. 3. A. Representative physical property details of a single correlative turbidite along 280 km of margin parallel to the NSAF. See Fig. 1 for core locations. Along-strike series shows typical variability of the same event in five separate channels above any channel confluences. B. Representative physical property series of a single turbidite from proximal to distal position along 74 km of Gualala Channel. This example shows the merging of separate pulses with distance from the source.

large events in all cores, and many other events follow similar size patterns across the margin. We observe similar patterns along the NSAF margin, where size trends, and individual characteristics persist over large distances. Fig. 3B also shows the evolution of a single event down channel over a distance of 74 km, showing the gradual merging of two sand pulses into a bimodal grain distribution. Stratigraphic correlation of this type has the potential to establish stratigraphic links of individual events between core sites, independent of radiocarbon ages. Possible explanations for the correlation signatures are discussed in a subsequent section.

3.2.2. Radiocarbon analysis

To date the turbidites, we extract planktic foraminifera from the hemipelagic sediment below each turbidite. We do this because the boundary between the top of the turbidite tail and the hemipelagic sediment is difficult to identify, and bioturbation is concentrated at this boundary, possibly because the organic material brought down in the turbidite tail results in a benthic "bloom" [66]. To evaluate the effect of foraminifera shell size on the radiocarbon age in a single sample, we divided the foraminifers into large ($>\sim$350 μm) and small ($<\sim$350 μm) groups. The resulting ages are within 45 radiocarbon years of each other, suggesting foraminifer size is not a factor. The close match in ages between land and marine events observed in both Cascadia and on the NSAF also suggests that neither bioturbation [67,68] nor basal erosion significantly biases ^{14}C ages derived from planktic foraminifers.

To correct the ages for the thickness of the sample, we determined hemipelagic thickness between turbidites using visual observations of color change, X-radiography, mineralogic content, and high-resolution physical property data (Fig. 2). We also examined all turbidite bases to estimate the degree of basal erosion. An erosional index (EI) was estimated by examining the morphology of the turbidite bases, which can tell us that erosion occurred, though it may not correlate with the amount of erosion, and may miss laminar erosion. We then averaged the thicknesses determined from multiple methods, and averaged the two or three thickest layers out of a typical four at a given site. We infer that differential erosion is the most likely source of variability at any site, and by taking the thickest layers we attempted to reduce its influence. By averaging the thickest layers we also reduce the effect of variance in observations, which ranges between +/−0.5 to 1 cm.

Using a moving window average sedimentation rate, we corrected the original AMS ages by subtracting the time corresponding to the thickness of the sample interval. Hemipelagic thickness was then converted to time for input into OxCal calibration software [69,70]. A sedimentation rate regression analysis was employed to flag erosion at a given interval, and provide a check for consistency downcore, as sudden hemipelagic sedimentation rate changes in the marine environment are relatively rare (see Elect. Supl). Outliers in this analysis are most likely caused by basal erosion because ages appear to be older, with less sediment thickness between events than expected.

Fig. 4 illustrates the main steps used to combine ^{14}C age and hemipelagic sedimentation constraints. Since the calculated sedimentation rates are also dependent on the radiocarbon ages, and on basal erosion, there is some unavoidable circularity in this process, however analysis of multiple cores at each key site can address these issues quite well.

We used the Bayesian methods within OxCal to take advantage of multiple ages (if within analytical error of one another), include constraints imposed by the time represented by hemipelagic sediment between events, and in one case used historical information to restrict ages. Where age data are missing, sedimentation rates alone can be used to model event ages, which we have done for several events in our time series due to scarcity of foraminifers in those intervals.

Fig. 4 shows a detailed example using OxCal with hemipelagic sedimentation and historical constraints for the 1906 and the penultimate earthquakes. Using this well-known event, and time constraints provided by the hemipelagic sediment deposited in the interseismic period, OxCal returns the calendar age of the 1906 earthquake to within a few years (Fig. 4). The penultimate event is similarly constrained to a narrower time window than obtained by simple calibration.

The age constraints provided by uniform sedimentation between events are quite strong, in fact somewhat too strong, since the inter-event hemipelagic sediment can account for nearly 100% of the time in a given core (the turbidites themselves representing zero time). While this is good, in a statistical sense, there is no temporal "room" left for the probability density function (PDF) required to describe the ^{14}C event age. For this reason, we presently relax the hemipelagic constraint to 75% of the time represented to allow for overlap of the hemipelagic time interval with the PDF for each turbidite age in OxCal.

In our age series, we apply a reservoir correction that is linearly interpolated between the nearest points

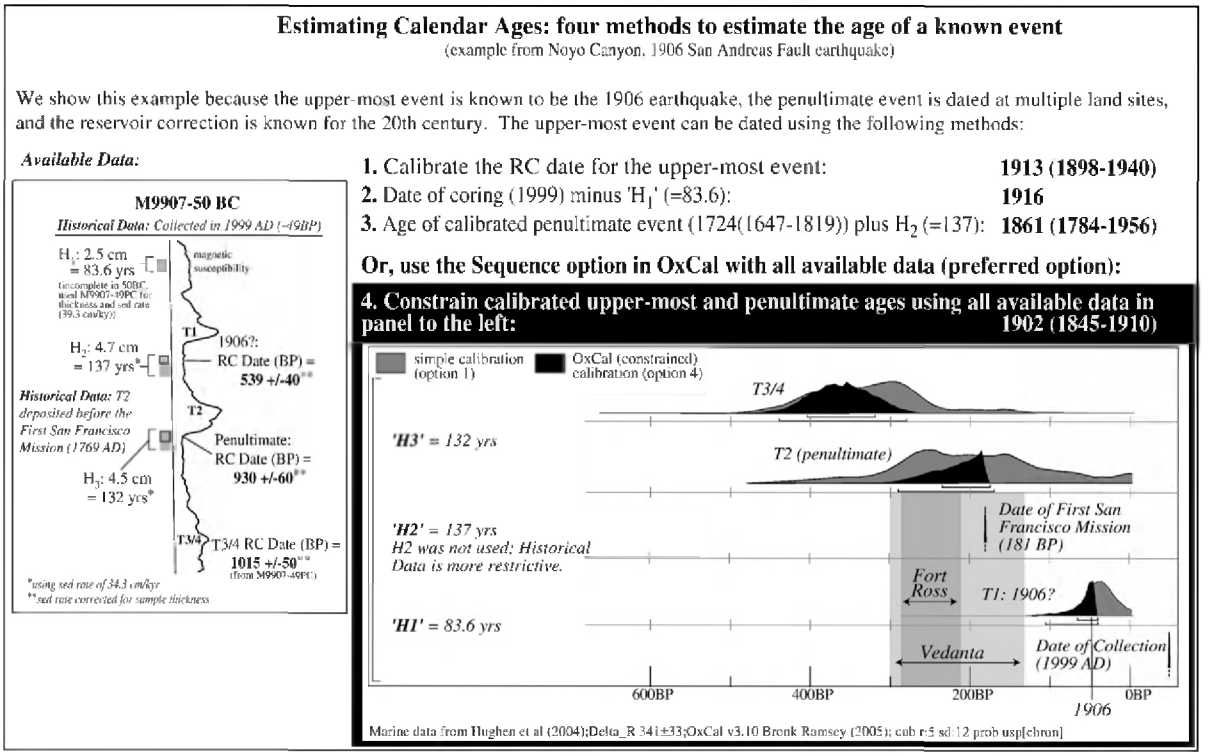

Fig. 4. OxCal methods test using the well constrained 1906 earthquake and associated paleoseismic data onshore and offshore. The left panel shows the hemipelagic (H) data determined from visual observation, physical property data mineralogy and x-radiography. H data is then input to OxCal and with raw ^{14}C ages are converted to time via sedimentation rate curves developed for each site. Right panel shows four ways to calculate the age of the 1906 earthquake, with the preferred method being the use of underlying and overlying hemipelagic intervals, historical data (no written record of an earthquake between the date of the first San Francisco Mission built in 1769 and 1838), and ^{14}C ages together. This method yields 1902 (1845–1910) for the 1906 event. The Fort Ross and Vedanta mean age and range for the penultimate event is shown, along with the OxCal solution for that event, calculated using the preferred method. The turbidite result 1660–1769 (~1760 peak) for the penultimate event is in good agreement with NSAF paleoseismic sites on land: Fort Ross=1710 (1610–1810), Vedanta=1711 (1695–1720) [28,32].

available in the Marine04 database [71], which are at San Francisco (ΔR 271+/−) and Coos Bay (ΔR 402+/−). Because the database is largely limited to the 20th century, time variation of the reservoir age is usually ignored because little data on the time history is available. We do not yet know whether time and space variable reservoir age issues will be significant offshore northern California, however we suspect it will show similar variability as along the Cascadia margin [72–74].

4. Results: Northern San Andreas turbidite record

4.1. Confluences and mineralogy

Fig. 2 shows the stratigraphy of two typical NSAF turbidites in core 24GC below several confluences of Viscaino, Noyo, and Gualala Channels (confluences "A", "B", and "C" in Fig. 1). At this site, we find that the multiple coarse pulses which also reveal the heavy mineral assemblage from individual canyon sources, stacked vertically in order of arrival at the core site. The turbidites at this site also have no hemipelagic sediment between the sand pulses, indicating little time passage between deposition of each pulse (the alternative, removal by erosion, is possible, but would have to occur in each turbidite at every correlative site). Further downstream, we observe bimodal heavy mineral coarse fractions, with mineralogic peaks representing the separate provenance components (Fig. 3 [75,76]). Fig. 2 also shows the magnetic susceptibility trace for the same two correlative turbidites, upstream of the confluences, in core 13TC. We observe no significant change in the stratigraphy between these two sites, despite input from multiple sources at the confluences. Further downstream at the site of core 31PC, we find that individual turbidites have the same stacking of coarse pulses, but the provenance input is less distinct,

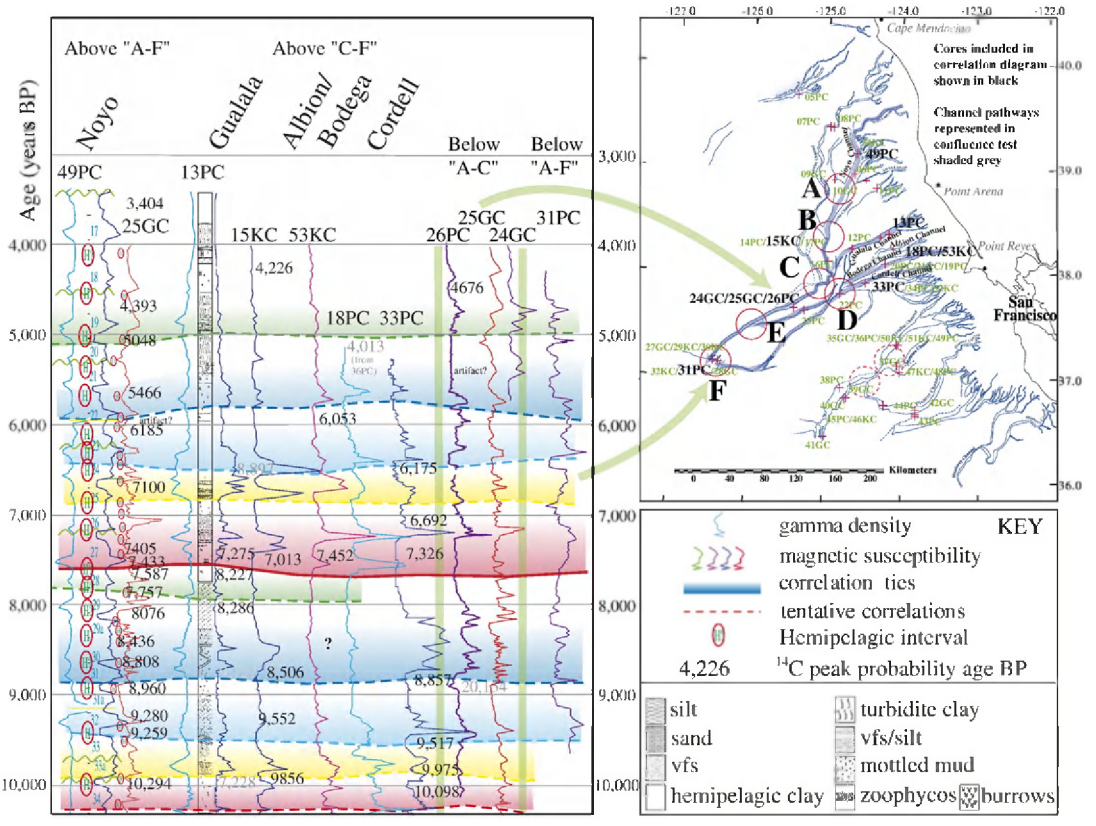

Fig. 5. "Confluence Test" as applied to the central NSAF margin channel systems for the period ~4000–10,000 ybp. Inset map shows eight confluences (southern two dashed, not yet tested). The correlation figure uses magnetic susceptibility records from six cores at four sites above confluence "C" (representative lithologic log for 13PC shown, 13PC gamma density shown in light blue). Magnetic susceptibility for three cores below confluence "C", and one core below confluences "A–F" are also shown. Green bars separate these three core sets, and are linked to the map. Core 25GC (red) also shown alongside 49PC with hemipelagic intervals (circled H) shown between turbidites. Magnetic trace for 49PC shows disturbance by sampling, density trace is shown for comparison. Mismatching hemipelagic intervals shown green, all others in red. Green wavy lines are known erosive bases. Turbidite numbers shown on 49PC in green. Peak radiocarbon ages are shown without ranges to reduce clutter, ranges are given for upper 14 events on Fig. 7. Color bands show correlation ties for key turbidites. While some details of each of the correlated turbidites vary from site to site as would be expected, the stratigraphy represented by these turbidites remains largely unaffected by passage through the confluences with other channels. The total number of turbidites is nearly constant, indicating that turbidite arrival at confluences from separate channel systems was most likely synchronous. See Fig. 6 for mag. sus. and density scales. Color scheme matches events in Figs. 6 and 7 for events common to both figures.

suggesting further mixing downstream. Fig. 5 shows our stratigraphic correlation detail for a series of cores upstream, near, and downstream of the confluences of Viscaino, Noyo, Gualala, Albion, and Cordell Channels. We show the time period from ~3500 ybp to ~10,000 ybp because the upper section is poorly preserved in some of the downstream cores. The downstream cores have, as yet, only a few dated turbidites, in part due to the low foram abundance at water depths in excess of 3500 m at these sites. The section ages are bounded by several late Pleistocene ages (not shown in Fig. 5), and the age of 4676 (4525–4810) ybp for T18 in core 26PC which we use to constrain the upper part of the correlation.

While additional ^{14}C ages are still needed, we can test for synchroneity by carefully matching events between upstream cores at Noyo and Gualala Channels and correlative events in the downstream cores in this time range. We matched the stratigraphy and checked for presence/absence of hemipelagic sediment between events (or an erosive event that removed it) as well as the multiple cues used in physical property correlation. We observe that upstream (49PC) and downstream cores (e.g. 25GC) both contain 22 events in this time range.

Differences between the two are minor, and appear mostly attributable to local basal erosion. Fig. 5 includes correlation with core 31PC, which is actually below a total of four confluences, with input from a total of six channels, while cores 24GC, 25GC, and 26PC each sample three channels. The good correlation between these cores suggests that input mixing at each confluence has little effect on the stratigraphy of the turbidites, even though the number of sources increases at each confluence. We infer that synchronous triggering is the only viable explanation for this, and are unable to suggest an alternative. Non-synchronous triggering should produce an amalgamated record that increases in complexity below each confluence, with only partial correlations for the synchronous events. The mixing and stacking of the provenance components further suggests synchronous arrival at the confluence. From these results we infer that the sites included in this analysis pass a strict test of synchroneity, and are most likely of earthquake origin. Further analysis of the remaining confluence sites is in progress. A similar use of mineralogic provenance to fingerprint source channels and test for earthquake origin has been used in the Sea of Japan by Shiki et al. [10].

4.2. Stratigraphic correlation

We have made a preliminary correlation of events along the length of the NSAF margin using subsurface correlation of the physical property logs as described above. This has been hampered somewhat by the fact that the turbidite signal for most of the NSAF channels is subdued by comparison to Cascadia. This is not surprising, given smaller earthquakes and greater epicentral distance to the canyons. The correlation is made within a ^{14}C age framework, with some vertical stretching of cores required due to varying sedimentation rates.

Fig. 6 shows the regional correlation of turbidite stratigraphy spanning the Holocene, and Fig. 7 shows the upper ~2100 yr of record, making use of high-resolution magnetic susceptibility data (3 mm spacing, point sensor). We focus here on the upper 2100 yr of the record; the analysis of earlier periods in the Holocene is the subject of ongoing investigation. Our Noyo Canyon cores, 49PC and companion Kasten core 54KC, are particularly important because unlike all the other channel systems, Noyo Canyon is actually cut by the NSAF, and has an epicentral distance of zero. Most likely for this reason, the turbidite record there is expanded in thickness, making investigation of the details of each event much clearer in those cores. Cores to the south have much reduced sedimentation rates, even though they are closer to the Russian River source, the largest river along the North Coast section of the NSAF. We speculate that the low hemipelagic sedimentation rates might be related to capture of much of the Russian River drainage and diversion into the San Joaquin Valley, which may have occurred during the Holocene [77]. By comparison to the robust Noyo record, most of the events along the NSAF in other channels are subdued, and indeed the upper 10 events shown in these figures are very fine silt turbidites not visible to the naked eye. Their unique signatures in the physical property data, however, allow good correlation between sites. We have collapsed a much larger set of core records onto the representative correlation diagrams shown in Figs. 6 and 7. A key stratigraphic datum in this correlation is T11, which is a robust event correlated and visible as a sandy turbidite in all cores, dated at 2574 (2397–2681) ybp in Noyo Channel, and 2256 (2080–2401) ybp in Gualala Channel. We suspected that the original ^{14}C age for this event (~2600 ybp) was too old (possible basal erosion) and have used constraints from hemipelagic sedimentation rates surrounding this interval to estimate the ~2100 ybp age in Fig. 7.

As in Cascadia, correlation of individual events based on the grain size distribution represented by the magnetic and density data are possible both along strike and down channel. Robust event "signatures" that can be recognized both within single channels, between multiple channel systems, and above and below confluences support the inference that they in fact represent the same source events, independent of other methods. We observe that the correlated events retain their essential character, typically made up of a stack of coarse pulses, for considerable distances along the margin. The "signatures" are observed to evolve downstream where coarse pulses merge with distance from the margin. The event "signatures" also evolve to some extent along strike in some cases, although in other cases stratigraphic sections at opposite ends of the fault system match as well as close neighbors. These properties can be observed through close inspection of Figs. 3–7.

4.3. Radiocarbon time series and comparison to onshore paleoseismic sites

In terms of event ages and their distribution in time, the youngest 15 events have a mean repeat time of ~200 yr, with a standard deviation of 60 yr. Using peak PDF values for event ages, the minimum interval value is ~95 yr between T7a and T7 and T12a and T12, and the maximum value is ~270 yr between T5 and T6 and

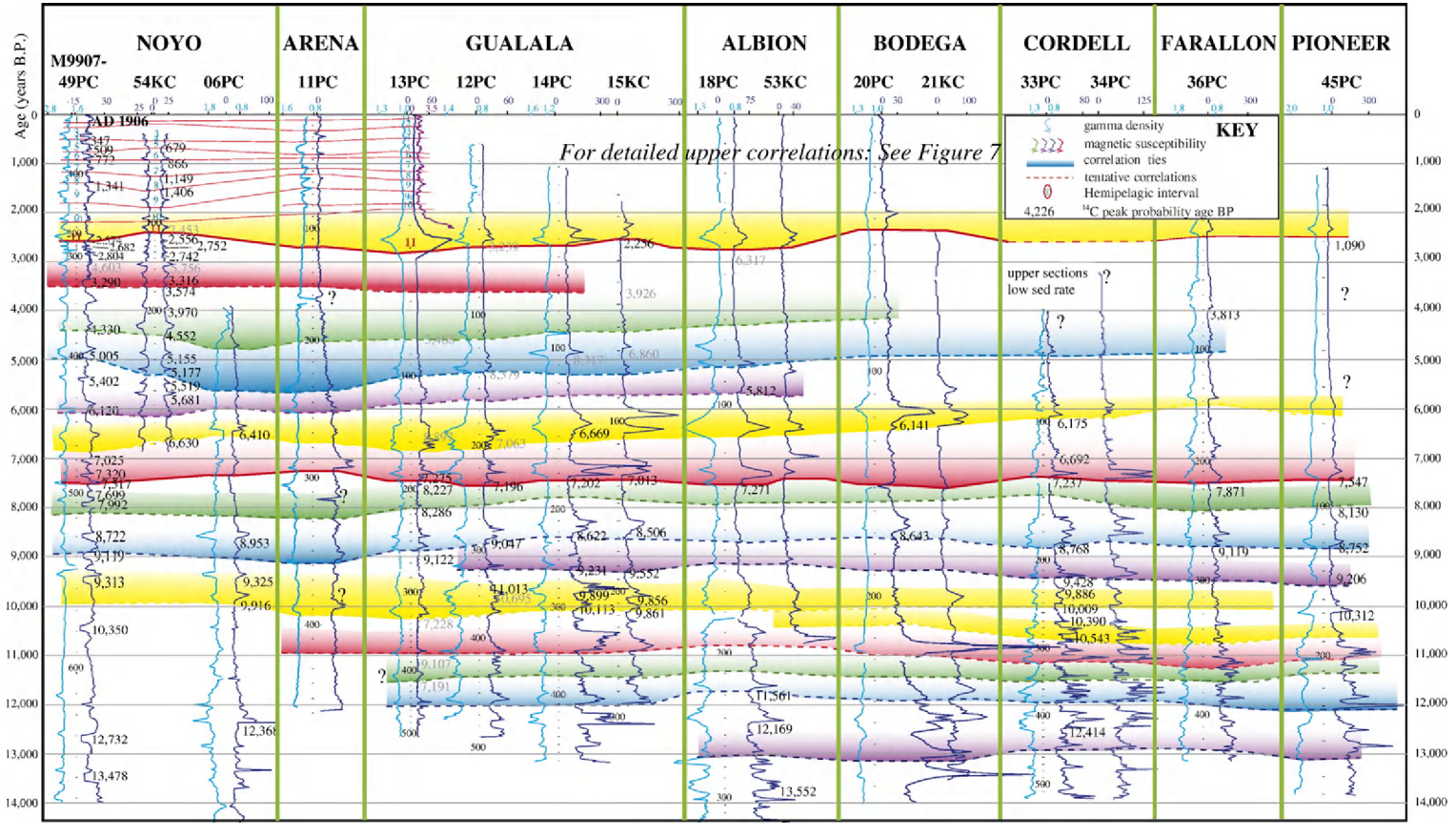

Fig. 6. In progress Holocene correlation diagram for NSAF system cores. Light blue traces are gamma density, dark blue traces are magnetic susceptibility (Kasten cores "KC" do not have associated density data as they are too large for the scanner). This correlation is approximately oriented in a ^{14}C age framework, with some vertical stretching of cores based on differing sedimentation rates. Peak probability calibrated ages corrected for sample thickness are shown in black (gray if questionable) below the dated turbidite, 2σ range omitted for clarity. Upper ~2500 years of data shown in Fig. 7 using 3 mm high-resolution magnetic susceptibility data. Significant correlation horizons, are shown, but not all individual events are depicted to reduce clutter. Color scheme matches events in Figs. 5 and 7 for events common to both figures.

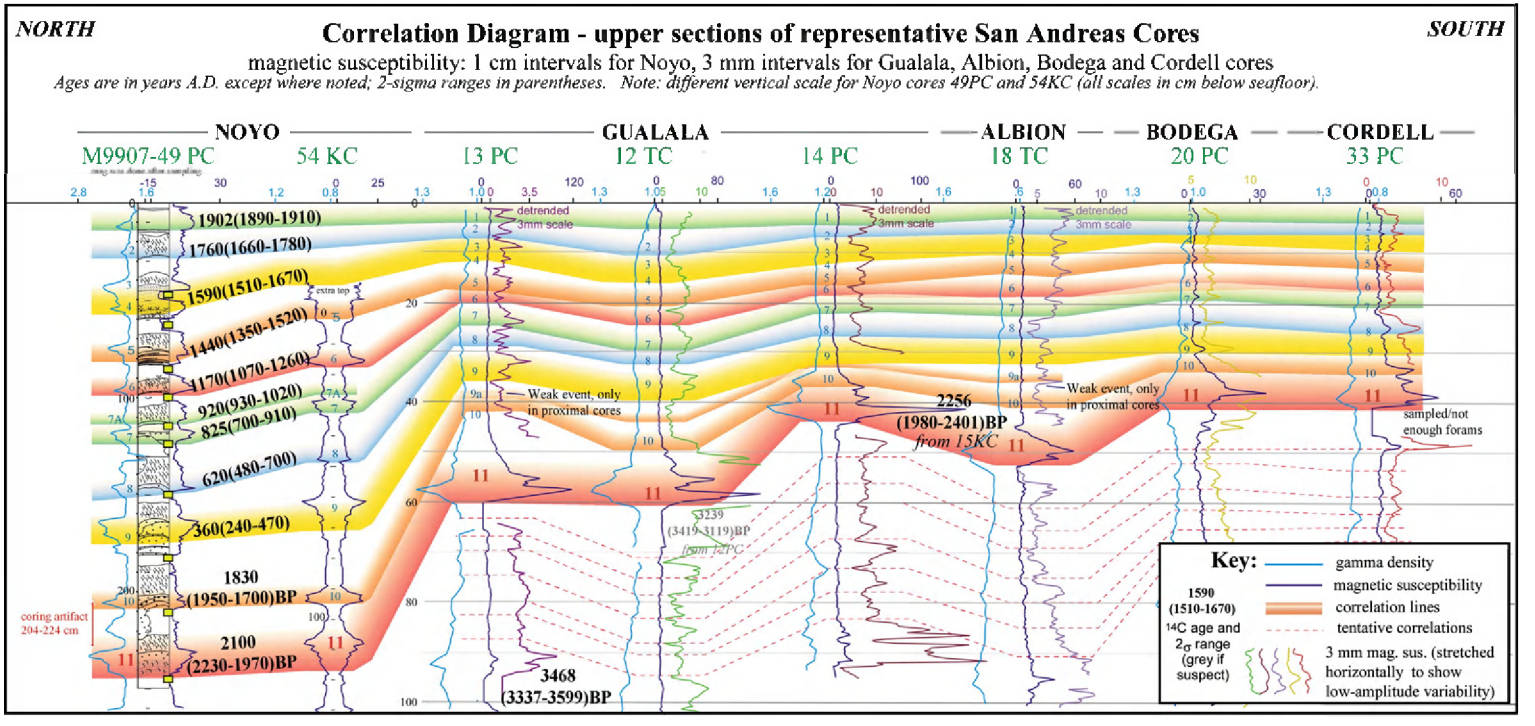

Fig. 7. Correlation diagram for the uppermost ~3000 years in NSAF system cores. Channel locations shown in Fig. 1. Light blue traces are Gamma density, dark blue are magnetic susceptibility. 1 cm resolution magnetic susceptibility data are shown for Noyo cores, and 3 mm high–resolution data are shown for all other cores. The 3 mm magnetic susceptibility data is stretched horizontally (variable colored traces) to show the low amplitude signal resolved with this resolution. Event numbers in blue at core centers. NSAF cores all have a number of relatively thick events that serve as excellent datums, and are the basis for our regional correlations in Fig. 6. The uppermost of these marker events, a very distinctive multipulse event dated at ~2100 ybp, is shown labeled "11" in red. Gualala, Albion, Bodega and Cordell and 54KC core tops have been vertically expanded for viewing to offset low sedimentation rates in the upper 2100 years for all cores. OxCal age peaks and ranges shown on cores 49PC and 54KC at left; these ages do not match Fig. 6 ages, for which data are insufficient for OxCal analysis. Gualala ages have been corrected for sample thickness only. Correlation for weak events T7a and T9a uncertain and not shown beyond Noyo Channel. T7a is datable, and included in our time series; T9a appears to be limited to two adjacent proximal core sites, and is not included in the recurrence statistics. 49PC high–resolution magnetic trace is punctuated by sample voids, indicated by yellow squares. Color scheme matches events in Figs. 5 and 6 for events common to both figures.

T10–T11 (we refer to the third event as "T3–4" because it is a doublet that may yet prove to be two events). We find these values reasonably consistent with previous paleoseismic data onshore. The ages shown in Fig. 8 include 11 ages reported by Zhang et al. [31] from the Vedanta Marsh site, and 5 ages reported by Kelson et al. [32] from sites at Fort Ross. These results indicate that the penultimate event occurred ~AD 1700–1750 north of San Francisco, and that the age correspondence is good for the last ~2300 yr when comparing Noyo Canyon marine ages to Vedanta and Fort Ross land ages. For a given time interval, we see approximately the

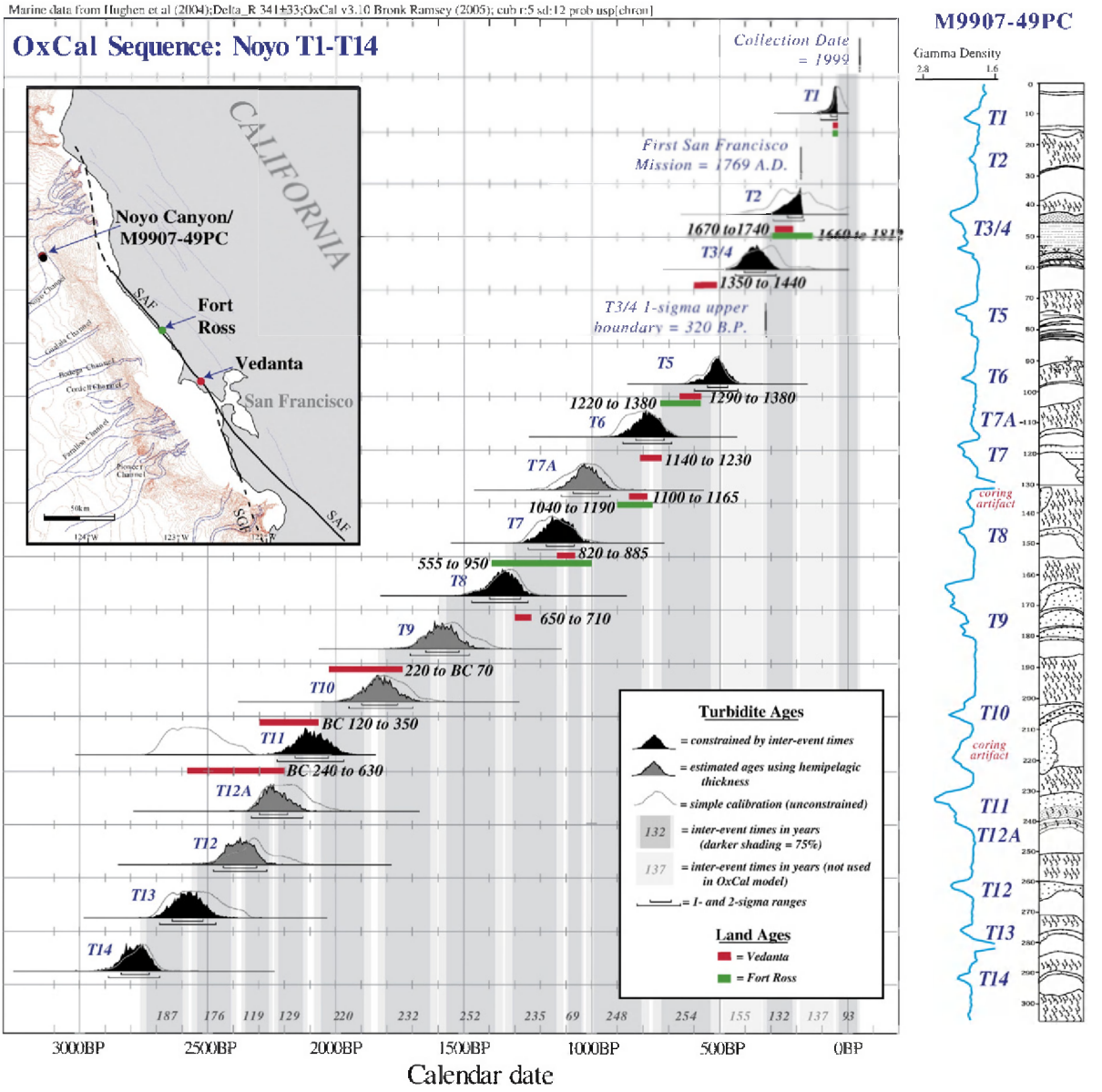

Fig. 8. OxCal age model for the youngest 15 events in the NSAF offshore system, and comparison to onshore ages. Inter-event times based on hemipelagic sediment thickness (represented by gray bars) were used to constrain original ^{14}C calendar age distributions (gray traces) using the SEQUENCE option in OxCal. Inter-event times were estimated by converting hemipelagic sediment thickness between each pair of events to time using the sedimentation rate. Events dated more than once were combined in OxCal prior to calibration if results were in agreement; if not in agreement, the younger radiocarbon age was used in the final model. Five ages are calculated from sedimentation rates where not enough forams were present for ^{14}C dating. The resulting probability distributions (filled black, gray for undated events) are mostly in good agreement with land ages from Fort Ross except for T3–4 and T7a (green lines; [32]) and Vedanta (red lines; [31]). See inset for geographic locations. See Electronic Supplement for OxCal input data and sedimentation rate curves.

same total number of events (±1) onshore and offshore, suggesting either a coincidence, or that land and marine sites are recording the same events. Further support for a linkage between the turbidite series presented here and onshore earthquakes, is the good correspondence between land and turbidite recurrence intervals, which are 200 yr and 230 yr for marine and land ages respectively. Individually, most ages except Noyo T3–4 (a doublet) and T7a have significant overlap of age ranges (Fig. 8). In addition, our event T3–4 was not reported at Fort Ross, and our event T9 was apparently not observed at Vedanta. Nevertheless, our preliminary stratigraphic correlation and age series, taken together, suggests that the previous 11 events may be correlated from Noyo Canyon to at least to the latitude of Vedanta, just north of San Francisco. If correct, our initial along-strike correlations imply rupture lengths for many (or most) events of >250 km.

5. Discussion

We infer that along-strike physical property correlations, supported by application of the "confluence test" and good correspondence with land paleoseismic dates both in individual matching, and total number of events, supports the use of offshore turbidites as paleoseismic indicators for the NSAF. We suggest several other lines of evidence that support this inference. First, the recurrence interval overall is consistent with other paleoseismic evidence from the North Coast segment of the fault, such as Prentice [30], Zhang et al. [31], and Kelson et al. [32]. Second, the mean recurrence interval changes abruptly (more than doubling) at the MTJ, from a value consistent with NSAF earthquakes south of the MTJ, to a value consistent with Cascadia earthquakes north of the MTJ [61]. We can think of no other reason for such a rate change, and indeed if such a change were due to external factors such as storm frequency or sediment loads, the frequency should increase northward, not southward as observed. Third, we observe that the thickness of the turbidites decreases southward as the shelf widens and the distance from the canyon heads to the fault increases (see Fig. 1). This occurs despite closer proximity to the main sediment sources, the Russian River and San Francisco Bay, which are to the south. This relationship suggests that epicentral distance, and not sediment supply, is the controlling factor for turbidite size, at least during Holocene high sea levels. This observation also supports our primary inference of earthquake origin, and is consistent with observations in Cascadia where robust turbidites are found in channels fed by small sediment sources, such as the Mendocino Channel fed by the Mattole River [78].

Physical property correlations often reveal detailed correlatable patterns that were unexpected. The magnetic-density event signatures we see are created by sand rich layers, mostly in the base of the turbidite. These layers include heavy (dark) minerals such as magnetite and hematite, which are largely responsible for the signatures. This is clear from the high-resolution imagery and X-rays, which show an obvious correlation between, density, magnetic susceptibility, and the coarse stringers in the turbidites [61] (Fig. 2). The correlation of these signatures indicates that the integrity of the signatures, and thus the pattern of coarse fraction deposition, is maintained to some extent over time and distance during the turbidity current. One might expect that such correlation could be due to details of how the turbidity current initiated in the canyon's upper reaches. An earthquake, unlike other triggers for submarine landslides, is likely to trigger multiple failures along the length of a canyon. Thus the turbidity current could contain multiple inputs, each containing a coarse fraction pulse, which coalesce down channel (this could also be due to retrograde landsliding). This could explain the persistent pattern we see within channels as reflecting an original multiple source input. But we are still left with the problem: Why do they correlate beyond an individual channel system, to other channels with different pathways?

The fact that they correlate at all is strong evidence that the turbidity currents were earthquake generated, and is robust regardless of the reasons for the correlation. Japanese investigators have similarly shown that the only plausible mechanism for multiple, simultaneous, regional landslide triggering, is an earthquake (see also [8]). We further suggest then that the only plausible commonality between correlative turbidites in separate channels is the original earthquake itself. In the case of the NSAF, we find that turbidites correlate across channels where the mineralogy is different, the physiography is different, the sediment sources are different, and the underlying geology is different. We postulate that the physical property signatures may record elements of the unique shaking signal imparted to the sediment failure region by the earthquake itself, in effect the physical property signatures may be crude paleoseismograms, imparting some information about magnitude, source character, or aftershocks to the depositional history of each turbidite [79,80]. This may be a controversial interpretation, but we are led to it out of a need to explain the observed data. This topic is the focus of another paper that makes use of both NSAF and Cascadia data (Goldfinger et al., in preparation), and will be tested experimentally in the near future.

The direct tie between events at widely separated sites implies, we infer, that this method can be used to link events separated in space directly, independent of but strengthened by ^{14}C dating. This method has the potential to overcome the largest issue in paleoseismology, the linking of events along strike via radiocarbon dating, with its inherent errors, to determine rupture length and segment recurrence values.

Our data, and those from Vedanta and Fort Ross, suggest an age near AD 1700–1750 for the NSAF penultimate event. While Vedanta and Fort Ross are sufficiently distant from Cascadia to preclude confusion, the Noyo Canyon offshore site is much closer at 90 km. The ^{14}C ages cannot distinguish the penultimate NSAF from the Cascadia AD 1700 event. However this event, as with most of the other 10 events discussed here, can be correlated well to the south, making it unlikely that the Cascadia record is confused in the NSAF record.

A related question of importance for the NSAF is the minimum magnitude and triggering distance from the earthquake hypocenter. Shiki et al. [10] observed that earthquakes less than Mw=7.4 do not trigger turbidity currents in the Japan Sea or Lake Biwa, and similarly cores taken before and after the 1992 Mw 7.1 Petrolia earthquake in the canyon source area do not include this event [78]. Several NSAF events that are well recorded in Noyo Channel are much more weakly represented in channels to the south, while others are robust in all channels. We suspect that there are probably smaller events not represented in the offshore data, and that they may similarly be unrepresented in the onshore data. Observations of turbidites from small events may also simply be a function of the resolution of the observations. We do not presently understand why some events such as T11 in the NSAF record, are much larger than others, particularly considering that the 1906 earthquake was likely near the maximum magnitude for that fault segment.

With a long paleoseismic record we can draw some preliminary conclusions about the distribution of recurrence intervals with time. A frequency histogram for the binned repeat intervals for the 15 earthquake series of Fig. 8 is shown in Fig. 9. While preliminary, this suggests the majority of repeat intervals lie between 150 and 250 yr. The minimum rupture lengths of ~320 km established from the turbidite data presented here imply magnitudes of 7.8–8.2 for these events based on empirical rupture length magnitude relationships [81]. Future work will test the full rupture length south of San Francisco for these events.

Finally, long paleoseismic records in both Cascadia and the NSAF offer many opportunities to investigate clustering and fault interaction. Given the close

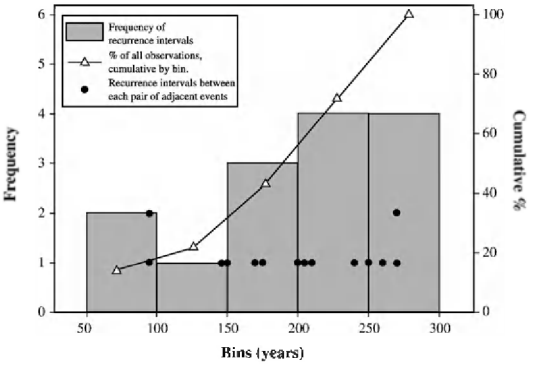

Fig. 9. Histogram showing the frequency of recurrence intervals within each bin (purple bars), with cumulative percent of all inter-event times (n=14) shown at the midpoint of each bar (circles filled in green). The actual data (black circles, each circle representing one recurrence interval) show the majority of recurrence times (8 out of 14) are between 150 and 250 years. (For interpreatation of the references to color in this figure legend, the reader is referred to the web version of this article.)

connection between the NSAF and Cascadia, it might be surprising if we did not see a temporal connection. The close temporal correspondence between the NSAF penultimate event ~AD 1700 and the Cascadia AD 1700 event is striking, and suggestive of stress triggering. Testing this hypothesis is the subject of ongoing investigation.

6. Conclusions

We have tested the turbidite record along the NSAF for synchronous triggering of turbidity currents as a method for determining the origin of these deposits, whether from earthquake, or other sources. We have used ^{14}C ages, relative dating tests at channel confluences, and direct correlation of physical properties to determine whether turbidites deposited in separate channel systems are correlative, that is, they were triggered by a common event. The NSAF late Holocene turbidite record examined thus far has passed these tests, and can be correlated with multiple proxies along multiple canyon systems from the MTJ to offshore San Francisco. The inference of earthquake origin is further supported by an abrupt change in turbidite recurrence interval at the Mendocino Triple Junction, from ~200 yr, a value consistent with onshore NSAF earthquakes to the south, to a value of ~520 yr consistent with the Cascadia subduction zone to the north.

Preliminary comparisons of our event ages with existing and in progress work at onshore coastal sites show good correspondence, further circumstantial evidence that the offshore record is primarily earthquake

generated. During the last ~2100 yr, we observe 11 most likely correlative turbidites, including one likely generated by the 1906 earthquake, that can be traced between Noyo Canyon, near the MTJ, and Cordell Channel near Point Reyes. Using combined constraints from physical property correlation, radiocarbon ages, and inter-event sedimentation, we conclude that it is likely that at least 8 of 11 events recorded both onshore and offshore in the past 2100 yr have rupture lengths of at least 250 km, and extend from the MTJ region to near the latitude of San Francisco.

Acknowledgements

We thank the officers and crew of the Scripps vessels R.V. Melville and Revelle. We thank the members of the 1999 and 2002 Scientific Parties: Mike Winkler, Pete Kalk, Antonio Camarero, Clara Morri, Gita Dunhill, Luis Ramos, Alex Raab, Nick Pisias Jr., Mark Pourmanoutscheri, David Van Rooij, Lawrence Amy, Churn-Chi "Charles" Liu, Chris Moser, Devin Etheridge, Heidi Stenner, Chris Popham, Claire McKee, Duncan McMillan, Chris Crosby, Susanne Schmid, Eulalia Gracia, Suzanne Lovelady, Chris Romsos, Vincent Rinterknecht, Rondi Robison, David Casas, Francois Charlet, Britta Hinrichsen, Jeremiah Oxford, Miquel Marin, Marta Mas, Sergio Montes, Raquel Villalonga, Alexis Vizcaino, Santiago Jimenez, Mayte Pedrosa, Silvia Perez, Jorge Perez, Andreu Turra, David Lamas, Himar Falcon, and Andres Baranco. We thank David Schwartz, Mary Lou Zoback, Tom Fumal, Tina Niemi and many others for insightful discussions on the NSAF, and two anonymous reviewers for numerous improvements to the paper. We gratefully acknowledge funding by the U.S. National Science Foundation, Earth Sciences Division, and the U.S. Geological Survey National Earthquake Hazards Reduction Program.

Appendix A. Supplementary material

Supplementary data associated with this article can be found, in the online version, at doi:10.1016/j.epsl.2006.11.017.

References

[1] R.S. Stein, G.C.P. King, J. Lin, Change in failure stress on the southern San Andreas fault system caused by the 1992 M 7.4 Landers earthquake, Science 199 (1992).

[2] S.N. Ward, S.D.B. Goes, How regularly do earthquakes recur? A synthetic seismicity model for the San Andreas fault, Geophys. Res. Lett. 20 (19) (1993) 2131–2134.

[3] B.F. Atwater, Evidence for great Holocene earthquakes along the outer coast of Washington State, Science 236 (1987) 942–944.

[4] A.R. Nelson, B.F. Atwater, P.T. Brobowski, L. Bradley, J.L. Clague, G.A. Carver, M. Darienzo, W.C. Grant, H.W. Krueger, R. Sparks, T. Stafford, M. Stuiver, Radiocarbon evidence for extensive plate boundary rupture about 300 yr ago at the Cascadia subduction zone, Nature 378 (1995) 371–374.

[5] C. Goldfinger, C.H. Nelson, J. Johnson, Holocene earthquake records from the Cascadia subduction zone and Northern San Andreas fault based on precise dating of offshore turbidites, Annu. Rev. Geophys. 31 (2003) 555–577.

[6] C. Goldfinger, C.H. Nelson, J.E. Johnson, Deep-water turbidites as Holocene earthquake proxies: the Cascadia subduction zone and Northern San Andreas fault systems, Ann. Geofis. 46 (2003) 1169–1194.

[7] J. Adams, Paleoseismicity of the Cascadia subduction zone: evidence from turbidites off the Oregon-Washington margin, Tectonics 9 (1990) 569–583.

[8] R.E. Karlin, M. Holmes, S.E.B. Abella, R. Sylwester, Holocene landslides and a 3500-yr record of Pacific Northwest earthquakes from sediments in Lake Washington, Geol. Soc. Amer. bull. 116 (1–2) (2004) 94–108.

[9] Y. Inouchi, Y. Kinugasa, F. Kumon, S. Nakano, S. Yasumatsu, T. Shiki, Turbidites as records of intense palaeoearthquakes in Lake Biwa, Japan, Sediment. Geol. 104 (1996) 117–125.

[10] T. Shiki, F. Kumon, Y. Inouchi, Y. Kontani, T. Sakamoto, M. Tateishi, H. Matsubara, K. Fukuyama, Sedimentary features of the seismo-turbidites, Lake Biwa, Japan, Sediment. Geol. 135 (2000) 37–50.

[11] T. Nakajima, Y. Kanai, Sedimentary features of seismoturbidites triggered by the 1983 and older historical earthquakes in the easterrn margin of the Japan Sea, Sediment. Geol. 135 (2000) 1–19.

[12] K.A. Kastens, Earthquakes as a triggering mechanism for debris flows and turbidites on the Calabrian Ridge, Mar. Geol. 55 (1984) 13–33.

[13] T.M. Niemi, Z. Ben-Avraham, Evidence for Jericho earthquakes from slumped sediments of the Jordan River delta in the Dead Sea, Geology 22 (1994) 395–398.

[14] M.E. Field, The submarine landslide of 1980 off northern California, U. S. Geol. Surv., Circ. 938 (1984) 65–72.

[15] N. Garfield, T.A. Rago, K.J. Schnebele, C.A. Collins, Evidence of a turbidity current in Monterey Submarine Canyon associated with the 1989 Loma Prieta earthquake, Cont. Shelf Res. 14 (6) (1994) 673–686.

[16] A. Grantz, R.L. Phillips, M.W. Mullen, S.W. Starratt, G.A. Jones, S.S. Naidu, B.P. Finney, Character, paleoenvironment, rate of accumulation, and evidence for seismic triggering of Holocene turbidites, Canada Abyssal Plain, Arctic Ocean, Mar. Geol. 133 (1996) 51–73.

[17] W.R. Dickinson, W.S. Snyder, The geometry of the triple junctions related to San Andreas transform, J. Geophys. Res. 84 (1979) 561–572.

[18] D.F. Argus, R.G. Gordon, Current Sierra Nevada–North America motion from very long baseline interferometry: implications for the kinematics of the western United States, Geology 19 (1991) 1085–1088.

[19] J.W. Sauber, W. Thatcher, S.C. Solomon, M. Lisowski, Geodetic slip-rate for the eastern California shear zone and the recurrence time for Mojave Desert earthquakes, Nature 367 (1994) 264–266.

[20] C.W. Jennings, New fault map of California and adjacent areas, Calif. Geol. 48 (2) (1995) 31–42.

[21] M.L. Zoback, R.C. Jachens, J.A. Olson, Abrupt along-strike change in tectonic style: San Andreas fault zone, San Francisco Peninsula, J. Geophys. Res. 104 (1999) 10719–10742.
[22] D.A. Castillo, W.L. Ellsworth, Seismotectonics of the San Andreas fault system between Point Arena and Cape Mendocino in northern California: implications for the development and evolution of a young transform, J. Geophys. Res. 98 (4) (1993) 6543–6560.
[23] Working Group on California Earthquake Probabilities, Earthquake Probabilities in the San Francisco Bay Region: 2003 to 2032: U.S. Geological Survey Open-File Report 03-214, 235 p., 2003.
[24] A.C. Lawson, The California Earthquake of April 18, 1906, report of the State Earthquake Investigation Commission: Carnegie Institution of Washington, Publication 87 Volumes I and II, 1908 (reprinted 1969), Washington, D.C.
[25] R.D. Brown, 1906 surface faulting on the San Andreas fault near Point Delgada, California, Bull. Seismol. Soc. Am. 85 (1) (1995) 100–110.
[26] C.S. Prentice, D.J. Merritts, E.C. Beutner, P. Bodin, A. Schill, J.R. Muller, Northern San Andreas Fault near Shelter Cove, California, Geol. Soc. Amer. bull. 111 (1999) 512–523.
[27] D.P. Schwartz, D. Pantosti, K. Okumura, T.J. Powers, J.C. Hamilton, Paleoseismic investigations in the Santa Cruz mountains, California: implications for recurrence of large-magnitude earthquakes on the San Andreas fault, J. Geophys. Res. 103 (8) (1998) 17985–18001.
[28] T.M. Niemi, N.T. Hall, Late Holocene slip rate and recurrence of great earthquakes on the San Andreas fault in northern California, Geology 20 (1992) 195–198.
[29] P. Segall, Integrating geologic and geodetic estimates of slip rate on the San Andreas fault system, Int. Geol. Rev. 44 (1) (2002) 62–82.
[30] C. S. Prentice, Earthquake Geology of the Northern San Andreas Fault near Point Arena, California: [Ph.D. thesis], California Institute of Technology, Pasedena, California, 252 p., 1989.
[31] H. Zhang, T. Niemi, T. Fumal, A 3000-yr Record of Earthquakes on the Northern San Andreas Fault at the Vedanta Marsh Site, Olema, California, Seismol. Res. Lett. 77 (2) (2006) 248.
[32] K. Kelson, A. Strieg, R. Koehler, K. Kang, Timing of late Holocene Paleoearthquakes on the Northern San Andreas Fault at the Fort Ross Orchard Site, Sonoma County, California, Bull. Seismol. Soc. Am. 96 (3) (2006) 1012–1028.
[33] P. Segall, M. Lisowski, Surface displacement in the 1906 and 1989 Loma Prieta earthquakes, Science 250 (1990) 1241–1244.
[34] W. Thatcher, G. Marshall, M. Lisowski, Resolution of fault slip along the 470 km long rupture of the great 1906 San Francisco earthquake, J. Geophys. Res. 102 (1997) 5353–5367.
[35] C.S. Prentice, D.J. Ponti, Coseismic deformation of the Wrights tunnel during the 1906 San Francisco earthquake: a key to understanding 1906 fault slip and 1989 surface ruptures in the southern Santa Cruz Mountains, California, J. Geophys. Res. 102 (1997) 635–648.
[36] K.B. Clahan, Paleoseismic characteristics of the San Andreas Fault, Woodside, California, MS thesis, San Jose State University, San Jose, CA, (1996) 96 pp.
[37] J.C. Clark, Neotectonics of the San Gregorio fault zone; age dating controls on offset history and slip rates, USGS NEHRP Final Technical Report, 1999.
[38] T. Fumal, T. Niemi, H. Zhang, High Resolution Paleoseismic Records at Three Sites on the Northern San Andreas Fault, Seismol. Res. Lett. 77 (2) (2006) 269.
[39] B.C. Heezen, M. Ewing, Turbidity currents and submarine slumps, and the 1929 Grand Banks earthquake, Am. J. Sci. 250 (1952) 849–873.
[40] D.S. Gorsline, T. De Diego, E.H. Nava-Sanchez, Seismically triggered turbidites in small margin basins: Alfonso Basin, Western Gulf of California and Santa Monica Basin, California Borderland, Sediment. Geol. 135 (2000) 21–35.
[41] R.W. Sternberg, Transport and accumulation of river-derived sediment on the Washington Continental Shelf, USA, J. Geol. Soc. Lond. 143 (1986) 945–956.
[42] C. Goldfinger, C.H. Nelson, Holocene recurrence of Cascadia great earthquakes based on the turbidite event record. Nature, in revision (2005).
[43] C.K. Sommerfield, D.E. Drake, R.A. Wheatcroft, Shelf record of climatic changes in flood magnitude and frequency, north–coastal California, Geology 30 (5) (2002) 395–398.
[44] P. Puig, A.S. Ogston, B.L. Mullenbach, C.A. Nittrouer, J.D. Parsons, R.W. Sternberg, Storm-induced sediment gravity flows at the head of the Eel submarine canyon, northern California margin, J. Geophys. Res. 109 (2004) C03019.
[45] C.K. Paull, P. Mitts, P.W. Ussler III, R. Keaten, H.G. Greene, Trail of sand in upper Monterey Canyon: offshore California, Geol. Soc. Amer. Bull. 117 (9–10) (2005) 1134–1145.
[46] O.S. Madsen, Spectral wave-current bottom boundary layer flows: coastal engineering 1994, Proceedings, 24th International Conference, Coastal Engineering Research Council/ASCE, 1994, pp. 384–398.
[47] S. Caires, A. Sterl, 100-yr return value estimates for ocean wind speed and significant wave height from the ERA-40 data, J. Climate 18 (7) (2005) 1032–1048.
[48] O.H. Pilkey, Basin plains; giant sedimentation events, Spec. Pap. Geol. Soc. Am. 229 (1988) 93–99.
[49] D.G. McCubbin, Barrier-island and strand-plain facies, in: P.A. Scholle, D. Spearing (Eds.), Sandstone Depositional Environment, The AAPG, Tulsa, Oklahoma, 1982, pp. 247–279.
[50] R. Lovlie, P. Van Veen, Magnetic susceptibility of a 180 m sediment core: reliability of incremental sampling and evidence for a relationship between susceptibility and gamma activity, in: P. Turner, A. Turner (Eds.), Palaeomagnetic Applications in Hydrocarbon Exploration and Production, Special Publication, vol. 98, Geological Society, London, 1995, pp. 259–266.
[51] K. Fukuma, Origin and applications of whole-core magnetic susceptibility of sediments and volcanic rocks from Leg 152, Proc. Ocean Drill. Prog., Sci. Results 152 (1998) 271–280.
[52] A.L. Abdelayem, K. Ikehara, T. Yamazaki, Flow path of the 1993 Hokkaido–Nansei–Oki earthquake seismoturbidite, southern margin of the Japan Sea north basin, inferred from anisotropy of magnetic susceptibility, Geophys. J. Int. 157 (2004) 15–24.
[53] G. St-Onge, T. Mulder, D.J.W. Piper, C. Hillaire-Marcel, J.S. Stoner, Earthquake and flood-induced turbidites in the Saguenay Fjord (Québec): a Holocene paleoseismicity record, Quat. Sci. Rev. 23 (2004) 283–294.
[54] J.T. Hagstrum, B.F. Atwater, B.L. Sherrod, Paleomagnetic correlation of late Holocene earthquakes among estuaries in Washington and Oregon, G3 5 (2004), doi:10.1029/2004GC000736.
[55] H. Iwaki, A. Hayashida, N. Kitada, H. Ito, S. Suwa, K. Takemura, Stratigraphic correlation of samples from the Osaka Bay off Kobe based on magnetic properties and its implication for tectonic activity of the Osaka-wan fault for the last 6300 yr, Eos Trans. - Am. Geophys. Union 84 (2004) (GP41C-0053 F554).
[56] M. Schnellmann, F.S. Anselmetti, D. Giardini, S.N. Ward, Prehistoric earthquake history revealed by lacustrine slump deposits, Geology 30 (12) (2002) 1131–1134.
[57] J.A. Lees, R.J. Fowler, P.G. Appleby, Mineral magnetic and physical properties of surficial sediments and onshore samples

from the southern basin of Lake Baikal, Siberia, J. Paleolimnol. 20 (2) (1998) 175–186.

[58] R.B. Wynn, P.P.E. Weaver, D.G. Masson, D.A.V. Stow, Turbidite depositional architecture across three interconnected deep-water basins on the north–west African margin, Sedimentology 49 (4) (2002) 669–695.

[59] C. Goldfinger, A. Morey-Ross, M. Erhardt, C.H. Nelson, J.E. Johnson, J. Guiterrez-Pastor, Cascadia great earthquake recurrence: rupture lengths, correlations and constrained OxCal analysis of event ages, Eos Trans. AGU 86 (2005) (Fall Meeting Suppl., Abstract T11A-0357.1).

[60] J. Rivera, E.B. Karabanov, D.F. Williams, V. Buchinskyi, M. Kuzmin, Lena River discharge events in sediments of Laptev Sea, Russian Arctic, Estuar. Coast. Shelf Sci. 66 (2006) 185–196.

[61] C. Goldfinger, A. Morey, M. Erhardt, C.H. Nelson, J. Gutierrez-Pastor, R. Enkin, A. Dallimore, Cascadia Great Earthquake Recurrence: Rupture Lengths, Correlations and Constrained OxCal Analysis of Event Ages, proceedings of the USGS Tsunami Sources Workshop, Diggles, Geist, and Lee, eds. (2006), CD-ROM, April 21 and 22, 2006.

[62] A. Dallimore, R.E. Thomson, M.A. Bertram, Modern to late Holocene deposition in an anoxic fjord on the west coast of Canada: implications for regional oceanography, climate and paleoseismic history, Mar. Geol. 219 (1) (2005) 47–60.

[63] C. Goldfinger, C.H. Nelson, E. Johnson, A. Morey, Physical property correlations and radiocarbon ages illuminate Cascadia earthquake recurrence patterns, Eos Trans. AGU 84 (46) (2003) (Fall Meet. Suppl., Abstract S42A-0144).

[64] A. Morey, C. Goldfinger, C.H. Nelson, J. Chaytor, J.E. Johnson, A. Ericsson, TI: turbidite based earthquake record along the Northern San Andreas Fault, Eos Trans. AGU 84 (46) (2003) (Fall Meet. Suppl., Abstract T51C-02).

[65] R.B. Wynn, D.G. Masson, Canary Islands landslides and tsunami generation, in: J. Mienert, J. Locat (Eds.), Proc. 1st int. Symposium on Submarine Mass Movements and their Consequences, Kluwer, Dordrecht, 2003, pp. 325–332.

[66] C.R. Smith, R.H. Pope, D.J. DeMaster, L. Magaard, Age-dependent mixing of deep-sea sediments, Geochim. Cosmochim. Acta 57 (1993) 1473–1488.

[67] R.A. Wheatcroft, Experimental tests for particle size-dependent bioturbation in the deep ocean, Limnol. Oceanogr. 37 (1992) 90–104.

[68] J. Thomson, G.T. Cook, R. Anderson, A.B. Mackenzie, D.D. Harkness, I.N. McCave, Radiocarbon age offsets in different-sized carbonate components of deep-sea sediments, Radiocarbon 7 (2) (1995) 91–103.

[69] C.B. Ramsey, Radiocarbon calibration and analysis of stratigraphy: the OxCal program, Radiocarbon 37 (2) (1995) 425–430.

[70] C.B. Ramsey, Development of the radiocarbon program OxCal, Radiocarbon 43 (2001) 355–363.

[71] P.J. Reimer, M.G.L. Baillie, E. Bard, A. Bayliss, J.W. Beck, C.J.H. Bertrand, P.G. Blackwell, C.E. Buck, G.S. Burr, K.B. Cutler, P.E. Damon, R.L. Edwards, R.G. Fairbanks, M. Friedrich, T.P. Guilderson, A.G. Hogg, K.A. Hughen, B. Kromer, F.G. McCormac, S.W. Manning, C.B. Ramsey, R.W. Reimer, S. Remmele, J.R. Southon, M. Stuiver, S. Talamo, F.W. Taylor, J. van der Plicht, C.E. Weyhenmeyer, IntCal04 terrestrial radiocarbon age calibration, 26–0 ka BP, Radiocarbon 46 (2004) 1029–1058.

[72] L. Ingram, Holocene climate change recorded in radiocarbon age differences between shell and charcoal from a shell mound near San Francisco Bay, Eos Trans. Am. Geophys. Union 78 (1997).

[73] L. Anderson, M.B. Abbott, B.P. Finney, Holocene climate inferred from oxygen isotope ratios in lake sediments, Central Brooks Range, Alaska, Quat. Res. 55 (2001) 313–321.

[74] R.T. Patterson, A. Prokoph, A. Dallimore, R.E. Thomson, D.M. Ware, C. Wright, Impact of abrupt Holocene climate change and solar cyclicity on fish population dynamics in the NE Pacific, Geolog. Soc. Amer. Abstr. Programs 33 (2001) 159.

[75] C. Goldfinger, C.H. Nelson, J.E. Johnson, M.A. Arsenault, A. Eriksson, E. Karabanov, J. Chaytor, Physical property correlations from Cascadia great earthquakes: what are they telling us about the triggering events? Eos Trans. AGU 85 (47) (2004) (Fall Meeting Suppl., Abstract OS21E-01).

[76] A. Morey, C. Goldfinger, C.H. Nelson, J. Chaytor, J.E. Johnson, A. Eriksson, Turbidite based earthquake record along the Northern San Andreas Fault, Eos Trans. AGU 84 (46) (2003) (Fall Meet. Suppl., Abstract T51C-02).

[77] J.D. Hopkirk, Endemism in Fishes of the Clear Lake Region of Central California, Contributions from the Museum of Vertebrate Zoology of the university of california, University of California Press, Berkeley, 1973 (135 pages and plates).

[78] C.H. Nelson, C. Goldfinger, J.E. Johnson, G. Dunhill, Variation of modern turbidite systems along the subduction zone margin of Cascadia Basin and implications for turbidite reservoir beds, Deep-water Reservoirs of the World, GCSSEPM 20th Annual Research Conference, 2001, p. 31.

[79] C. Goldfinger, C.H. Nelson, J.E. Johnson, Deep-water Turbidites as Holocene Earthquake Proxies: the Northern San Andreas Fault System, San Andreas Fault Workshop, USGS, Menlo Park California, 2004.

[80] C. Goldfinger, A. Morey, H. Nelson, Deep-water turbidites as Holocene earthquake proxies along the Northern San Andreas Fault system, Seismol. Res. Lett. 77 (2) (2006) 195–196.

[81] D.L. Wells, K.J. Coppersmith, New empirical relationships among magnitude, rupture length, rupture width, rupture area, and surface displacement, Bull. Seismol. Soc. Am. 84 (4) (1994) 974–1002.